Synthesis of Cs_3MnBr_5 Green Phosphors Using an Eco-Friendly Evaporative Crystallization Process

Sangwook Park, Minji Ko, Hyeng Jin Kim, Keyong Nam Lee, and Young Rag Do*

ACCESS | 📊 Metrics & More | 📖 Article Recommendations | 🅢🅘 Supporting Information

ABSTRACT: Green (G) and red (R) light-emitting materials, such as quantum dots, perovskite nanocrystals, and inorganic phosphor powders, owing to their excellent optical characteristics, have attracted researchers' attention as color-conversion materials for lighting and display applications. However, these materials contain environmentally harmful elements, such as Pb or Cd, and/or they are synthesized using environmentally harmful synthetic approaches and conditions, involving the use of organic solvents, high pressure, high temperature, harsh atmosphere, and long reaction time. In this study, as an eco-friendly synthetic approach to synthesize lead-free Cs_3MnBr_5 G powder phosphor, we suggest an evaporative crystallization process of aqueous reactant solution. This synthetic process does not use toxic elements or solvents and the crystallization process utilizes only low reaction temperature and short reaction time under air atmosphere conditions. We successfully synthesized Cs_3MnBr_5 green powder phosphor, with excellent optical properties, by evaporative heating of a 200 nm syringe-filtered solution at 150 °C for 2 h. The synthesized Cs_3MnBr_5 phosphors have a photoluminescence quantum yield of 66.3%, a peak wavelength of 520 nm, a narrow bandwidth of 38 nm, and a photoluminescence decay time of 0.34 ms under blue excitation. This phosphor is expected to be a useful alternative G-emitting material that can compete with commercial green quantum dots, perovskite nanocrystals, or inorganic phosphors.
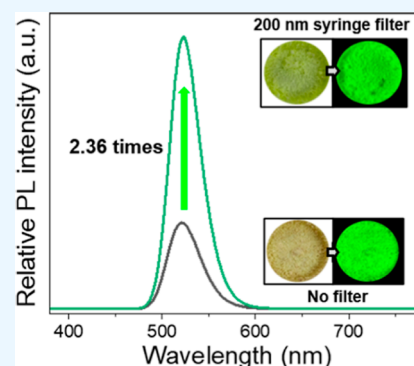
1. INTRODUCTION

During the last decade, highly efficient, narrow-band cesium lead halide perovskite $CsPbX_3$ (X: Cl, Br, I) nanocrystals (NCs) have been actively developed for use as red, green, and blue (RGB) emitters in backlight films of liquid crystal displays, as color-conversion layers in color-by-blue display devices, and as emitting layers of perovskite NC light-emitting diodes (PLEDs).[1−5] When these materials are used in display applications, their tunable peak position and narrow full width at half-maximum (fwhm) of the emission peak can be used to realize wide color gamut and high color purity. However, it is difficult to develop lead-free perovskite NCs or phosphors with appropriate peak position, narrow fwhm, and high photoluminescence (PL) quantum yield (PLQY).

Previously, because they have narrow fwhm of green emission peaks, Mn^{2+}-doped inorganic phosphors have been explored for application as backlights of liquid crystal displays. For example, γ-AlON/Mn^{2+}, Mg^{2+},[6] and $MgAl_2O_4$/Mn^{2+}[7] exhibit fwhm values of 44 and 35 nm, respectively. Furthermore, the fwhm value of $Sr_2MgAl_{22}O_{36}$/Mn^{2+} phosphor[8] can be as low as 26 nm and that of $ZnAl_2O_4$/Mn^{2+}[9] can be as low as 18 nm. Although Mn-doped phosphors achieve narrow fwhm of the green emission peak, the parity-forbidden property of low-concentration-doped Mn activators leads to relatively low absorption and long PL decay time. Therefore, it is necessary to develop eco-friendly Mn-emitting G phosphors

with good peak position, narrow-band fwhm, relatively high doping level, and relatively short PL decay time.

Fortunately, recently developed zero-dimensional (0D) metal halides provide longer distance between Mn^{2+} ions, which enables spontaneous emission with narrow-band G, R color.[10−12] In addition, these materials also have relatively fast PL decay time, from a few nanoseconds to a hundred microseconds, making them appropriate for display applications. The d−d transitions of Mn^{2+} ions in isolated tetrahedral and octahedral crystal fields are the sources of the pure G and R emissions, respectively. In an earlier research, organic−inorganic 0D Mn^{2+}-based halides were reported as excellent candidates for narrow-band green emitters, with high PLQY and fast decay time.[13−15] However, the poor environmental stability of their organic-based composition limits their use in display applications. Recently, other groups have suggested the development of all-inorganic Mn^{2+}-based halides to form narrow-band G, R emitters for color-by-blue display applications;[16−21] such materials have relatively high PLQY,

**Table 1. Previous Work for the Synthetic Method of Cs_3MnBr_5 and $CsMnBr_3$ Phosphors**

formula	synthetic method	morphology	temperature (°C)	solvent	decay time (τ)	Color coordinates CIE x	CIE y	peak wavelength (nm)	fwhm (nm)	PLQY (%)	refs
Cs_3MnBr_5	evaporative crystallization	powder	boiling	HBr ethyl alcohol	290 μs	0.149	0.756	520	42	49	16
	LARC	powder	freezing	distilled water ethanol	290 μs			520	39	74.9	17
	hot-injection method	NC	200	1-octadecene (ODE), oleic acid (OA), oleylamine (OLA)	31.4 μs	0.172	0.684	520	43	48	18
	hot-injection method	NC	250	ODE, OA, OLA	210 μs			520	65	38	19
$CsMnBr_3$	mechano-synthesis	powder	200								20
	hot-injection method	NC	120	ODE, OA, OLA	605 ps			643		54	21
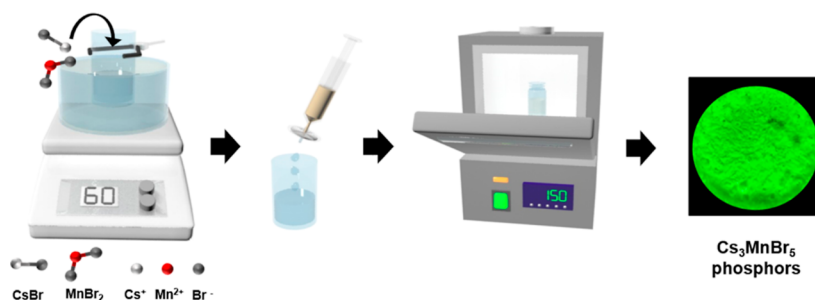
Figure 1. Schematic diagram of Cs_3MnBr_5 phosphors synthesized through evaporative crystallization.

excellent stability, and relatively short radiative PL decay times. In this regard, quite recently, cesium manganese(II) halide NCs and phosphors have attracted researchers' attention for use as eco-friendly G, R emitters with strong PL. Among various inorganic cesium manganese(II) halide phosphors, Cs_3MnBr_5 NCs and/or phosphors are promising G emitters to replace both transition metal Mn^{2+}-activated green phosphors and $CsPbBr_3$ NCs.

Cs_3MnBr_5 NCs and powder phosphors have been reported to show a strong green emission peak at 520 nm, with a narrow fwhm of 39−43 nm and a fast PL decay time of 290 μs. So far, the maximum PLQYs of Cs_3MnBr_5 powder phosphors and NCs have reached 74.9[17] and 48%,[18] respectively. As summarized in Table 1, both Cs_3MnBr_5 G and $CsMnBr_3$ R powders are synthesized using various crystallization approaches, such as HBr solution-based evaporative crystallization,[16] lyophilization-assisted recrystallization (LARC),[17] and a mechano-solid state reaction.[20] Cs_3MnBr_5 and $CsMnBr_3$ NCs are commonly synthesized using a hot-injection process.[18,19,21]

Except for LARC, most synthetic methods use environmentally harmful organic solvents. Although LARC is an eco-friendly approach, it requires a low-temperature freezer and long reaction time for the solid-to-gas phase transition.[17] After purifying the reactant ($MnBr_2$ and CsBr) solution using a silicon nitride (SiN_x) membrane nanofilter, we reported the synthesis of Cs_3MnBr_5 G phosphors using the evaporative crystallization process without any environmentally harmful materials such as organic solvents or acids. We reported PLQYs of Cs_3MnBr_5 green phosphors up to 53%.[22] However, our previous report did not focus on evaporative crystallization for Cs_3MnBr_5 G phosphors, but mainly on the fabrication of the SiN_x membrane nanofilter and the ultrafiltration process.

We introduced Cs_3MbBr_5 phosphor synthesis only as a good example of ultrafiltration by the SiN_x membrane nanofilter.

It is thus necessary to study the degree to which the purification process involving eco-friendly synthetic route of liquid-to-solid crystallization of aqueous reactant solution improves the purity, crystallization, and PLQY value of lead-free Cs_3MnBr_5 G phosphors. Furthermore, while performing evaporative crystallization processes, it is necessary to investigate the effects of various synthetic variables, such as reaction temperature, reaction time, and composition ratio, on the crystallization processes of Cs_3MnBr_5 green phosphors. In this study, using pre-purification of reactant solutions and optimization of synthetic variables, we have attained bright Cs_3MnBr_5 powder phosphors with a PLQY of 66.3%, a peak wavelength of 520 nm, and a fwhm of 38 nm by the evaporative crystallization process. The synthesis of Cs_3MnBr_5 phosphors starts with purification of the aqueous reactant solution. Undissolved ultrasmall-sized impurities are filtered using polyvinylidene difluoride (PVDF) syringes with pore sizes of 200 nm. Then, to obtain high-purity and crystalline Cs_3MnBr_5 G powder phosphors, the filtered solution is crystallized using phase transformation of liquid-to-solid. In this study, bright and lead-free Cs_3MnBr_5 G phosphor can be obtained using an eco-friendly water-based evaporative crystallization process with relatively low reaction temperature and short reaction time. Our successful development and detailed study of this eco-friendly synthetic route proves its potential to produce bright, lead-free, and narrow-band Cs_3MnBr_5 G phosphors for display applications.

2. RESULTS AND DISCUSSION

Cs_3MnBr_5 G phosphors are synthesized by heating an aqueous reactant solution of $MnBr_2$ and CsBr at a reaction temperature
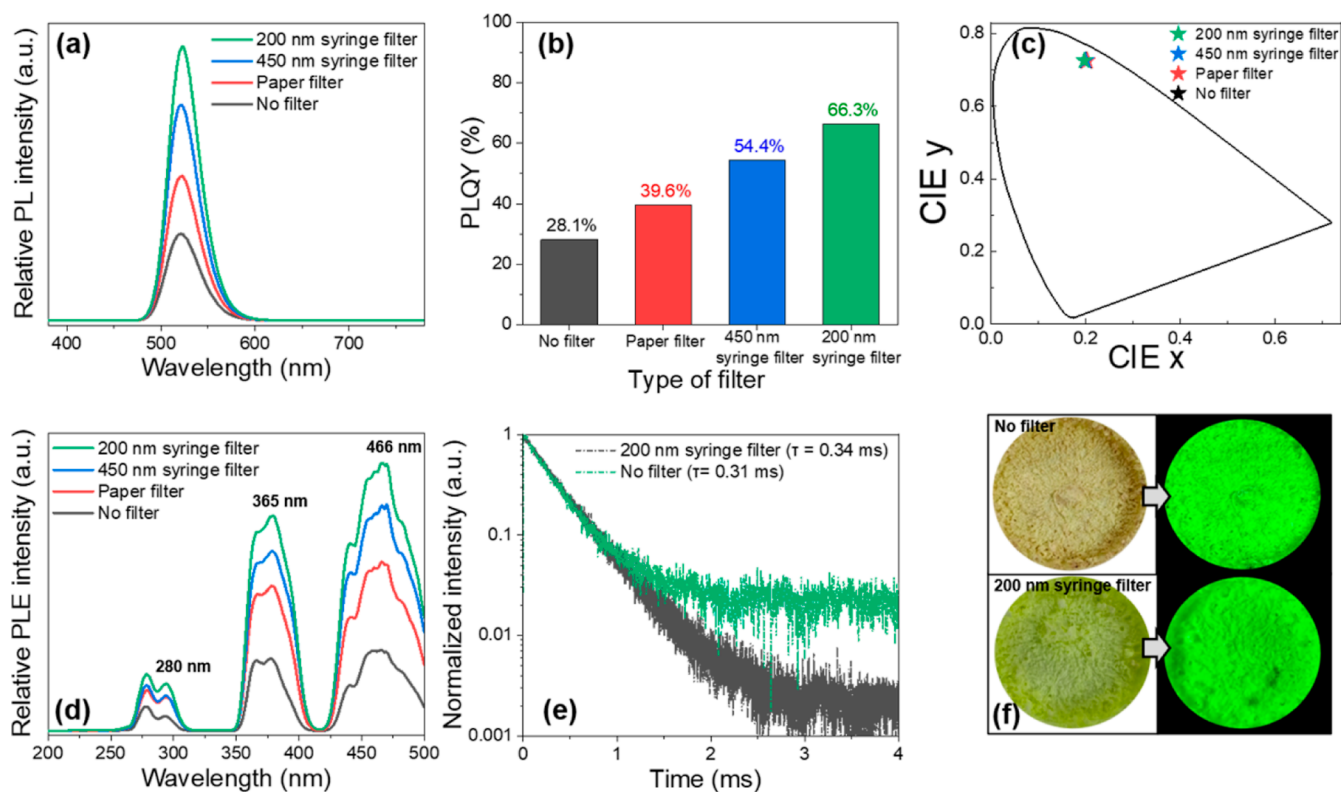
Figure 2. (a) PL spectra, (b) PLQY, (c) CIE color coordinates, (d) PLE spectra, and (e) time-resolved PL (TRPL) decay curves of the synthesized Cs_3MnBr_5 phosphors with various filtration conditions. (f) Photographs of the synthesized Cs_3MnBr_5 phosphors with no filtration and a 200 nm syringe filter before and after UV light (λ = 365 nm) irradiation.

below 200 °C through evaporative crystallization, as shown in the schematic diagram in Figure 1. To optimize the synthetic variables and select the best reactant materials, we assess the PLQY of the as-synthesized Cs_3MnBr_5 powder phosphors. Figure 2a compares the emission spectra of Cs_3MnBr_5 powders as synthesized under the various filtration conditions, which include non-filtration, paper filtration, and PVDF syringe filtration with pore sizes of 200 and 450 nm. When $MnBr_2$ is dissolved in distilled water, an environment in which manganese oxide or manganese hydroxide impurities may form can be created.[26] It is necessary to filter the reactant solution to reduce undissolved impurities, including oxygen impurities. Therefore, the PLQY of the synthesized Cs_3MnBr_5 phosphor increased as the filtration size became smaller, as shown in Figure 2b. Furthermore, the crystallinity of the Cs_3MnBr_5 phosphor obtained using the 200 nm filter was better than that obtained when not using any filter. During the purification step, we remove unnecessary impurity residue from aqueous reactant solutions before evaporative crystallization of Cs_3MnBr_5 powder phosphors.

After removing impurities from the two mixed reactant solutions, the PLQY of the purified and heat-treated Cs_3MnBr_5 powder phosphors increases from 35% for the non-filtered material to 66.3% after filtering using the 200 nm PVDF syringe filter. As expected, the smaller the pore size of the syringe filter used, the better the obtained PLQY (Figure 2b) of the Cs_3MnBr_5 powders. Therefore, we select a PVDF syringe filter with a 200 nm pore size, the smallest commercially available syringe pore size, for further study to optimize the optical quality of Cs_3MnBr_5 powder phosphors. As shown in Figure 2a, the strong G emissions of all as-synthesized Cs_3MnBr_5 phosphors originate from the d−d-

transition of the tetrahedrally coordinated Mn^{2+} ion with d^5 configuration. The CIE color diagram (Figure 2c) shows that all filtered and non-filtered Cs_3MnBr_5 powders have similar color coordinate values, indicating that the impurity phases have little effect on the emission spectrum. The identical normalized PL emission spectra, peak positions (∼520 nm), and fwhm's (∼38 nm) of the four Cs_3MnBr_5 powders also confirm that the radiative recombination processes had the same origin (Figure S1a,b). These results also confirm that impurities do not change the luminescence mechanism, but simply increase the non-radiative recombination, thereby reducing PLQY. The color coordinate values (x = 0.199 and y = 0.728) of the strongest PL emission spectrum indicate that Cs_3MnBr_5 powder phosphor has excellent G color and high color purity for display applications, comparable to those of previously reported Mn^{2+}-activated metal oxide phosphors. Figure 2d shows that the PL excitation (PLE) spectra are well matched with those of previously reported Cs_3MnBr_5 powder phosphors.[16−18] These PLE spectra are also monitored at emission levels of 520 nm. All PLE spectra show three similar bands at 280, 365, and 466 nm, which originate from the different levels of energy splitting of $^4T_1$ excited state under the tetrahedrally coordinated environment in the Cs_3MnBr_5 crystal structure. As shown in Figure S2, the narrow-band and green emission peak wavelength at 520 nm originates from the excitation of the lowest state of $^4T_1$ to the ground state of $^6A_1$.[25] Normalized PLE spectra of all four samples (Figure S1c) also have identical shapes and similar levels of intensity. The intense bands of the main excitation peaks, centered at 280, 365, and 466 nm, correspond to three excitation processes of
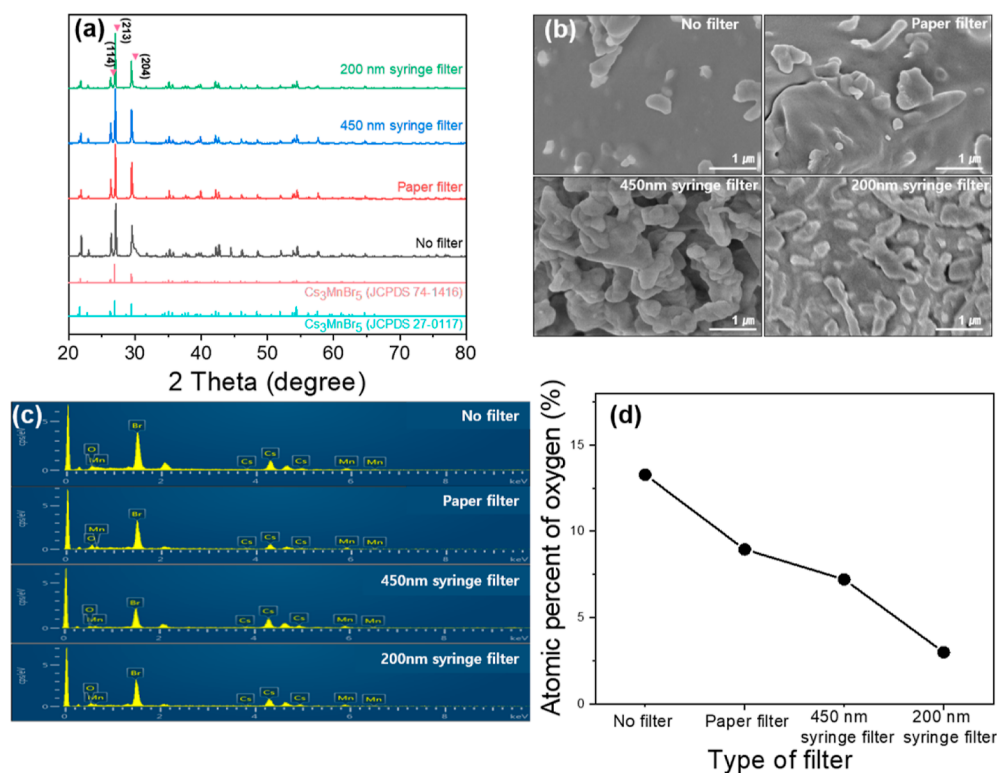
Figure 3. (a) XRD patterns, (b) scanning electron microscopy (SEM) photographs, (c) energy dispersive spectroscopy (EDS) spectra of Cs_3MnBr_5 phosphors synthesized under various filtration conditions, and (d) EDS data of elemental oxygen remaining with Cs_3MnBr_5 phosphors for various filtration conditions.

$^6A_1 \rightarrow {}^4F$ (UV B), $^6A_1 \rightarrow 4D$ (UV A), and $^6A_1 \rightarrow 4G$ (blue) transitions.[23,24]

These results indicate that Cs_3MnBr_5 powder phosphor can be excited by blue LED chips as well as UV A and UV B LED chips.

Figure S2 shows splitting energy levels and optical transitions for the tetrahedrally coordinated Mn^{2+} ion. The detailed light absorption, non-radiative relaxation, and green emission process of tetrahedrally coordinated Mn^{2+} ion in Cs_3MnBr_5 powder phosphors can be seen. Likewise, syringe-filter-purified Cs_3MnBr_5 phosphors can be used as good color-converting materials for color-by-blue and color-by-UV display applications. Figure 2e provides TRPL decay curves of the radiative emission bands at 520 nm obtained from non-filtered and 200 nm syringe-filtered samples. The TRPL decay curves of all samples can be fitted using a single exponential decay formula

$$I(t) = I_0 + A \cdot \exp(-t/\tau)$$

where $I(t)$ and I_0 are the intensities of PL emission at time t and $t \gg \tau$, A is a constant, and τ is the TRPL decay time for the exponential component. The PL lifetime of the Mn^{2+} d−d transition is particularly sensitive to the Mn−Mn distance. This is an important factor determining the PL lifetime, which can range from nanoseconds to milliseconds. The elongated Mn−Mn distance can lead to a coupled vibronic state such as self-trapped excitation, which is the cause of long, microsecond-scale lifetime.[18] The TRPL decay times for both types of non-filtered and filtered Cs_3MnBr_5 powder phosphors are 0.31 and 0.34 ms, respectively, found by fitting the decay curves using a single exponential equation, confirming the single recombina-tion process of unique Mn^{2+} ion sites in the Cs_3MnBr_5

structure.[14] Compared to the TRPL decay time in excited states of high PLQY filtered sample, TRPL decay time in excited states of low PLQY unfiltered powders were slightly faster due to decreased radiative decay channels in lower efficiency samples. After filtration, TRPL results of Cs_3MnBr_5 powder phosphors indicate that G emission leads to a slight prolongation of PL decay time after removal of impurities. Therefore, the long PL decay time of the Cs_3MnBr_5 phosphor is intrinsically due to the long distance of Mn−Mn ions; the longer PL decay time of the purified Cs_3MnBr_5 phosphor is due to the reduced non-radiative recombination process, achieved by reducing secondary phases and defects by filtration of impurities.

The photographs on the left-hand side of Figure 2f show as-synthesized powders of both non-filtered and filtered Cs_3MnBr_5 samples. The body color of the phosphor changes from dark yellowish for the non-filtered powder to bright greenish for the filtered powders. The disappearance of dark spots indicates the decreased impurities in the phosphors after filtration. Similarly, the photographs on the right-hand sides of Figures 2f and S3 show that a brighter green emitting light can be obtained under a 365 nm UV lamp from the better filtered powder phosphors.

Figure 3a compares X-ray diffraction (XRD) diffraction patterns of crystal structures of the as-synthesized Cs_3MnBr_5 powder phosphors obtained with different filtration processes before the evaporative crystallization process. After using PVDF syringe with 200 nm pore size to remove impurities from the mixed reactant solution, the XRD peak intensity of the Cs_3MnBr_5 crystal phase becomes more prominent. The syringe filter's improvement of the crystal structure is confirmed by the near-disappearance of the peak intensity of
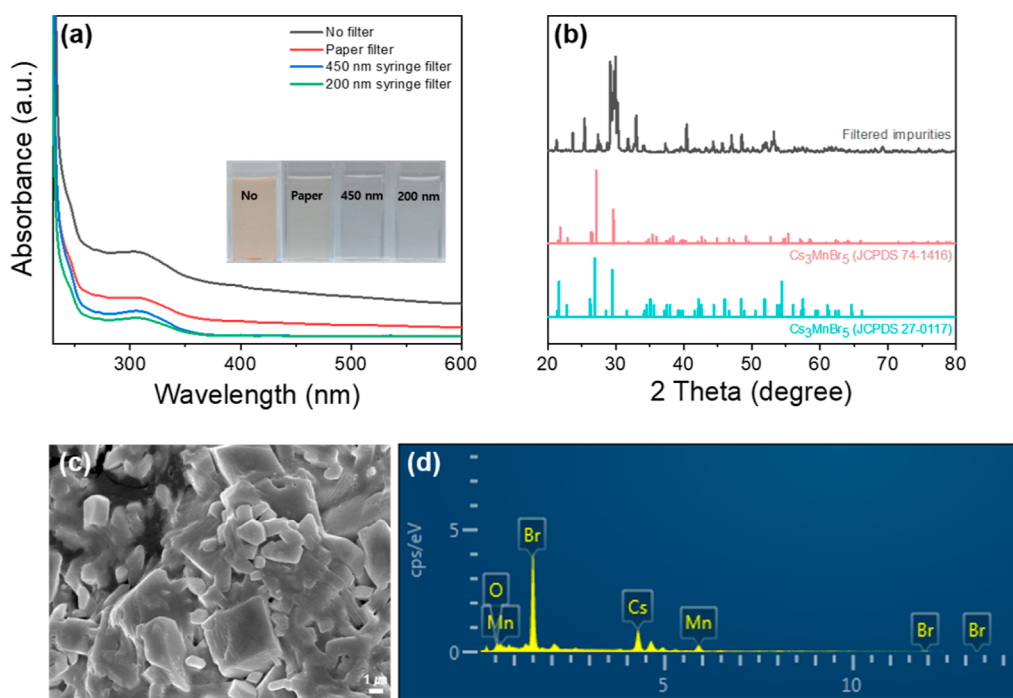
Figure 4. (a) Absorption spectra and photographs (inset) of solutions filtered under various filtration conditions and (b) XRD patterns of filtered impurities obtained from the surface of the 200 nm syringe filter. (c) SEM images and (d) EDS data of filtered impurities obtained with the 200 nm syringe filter.
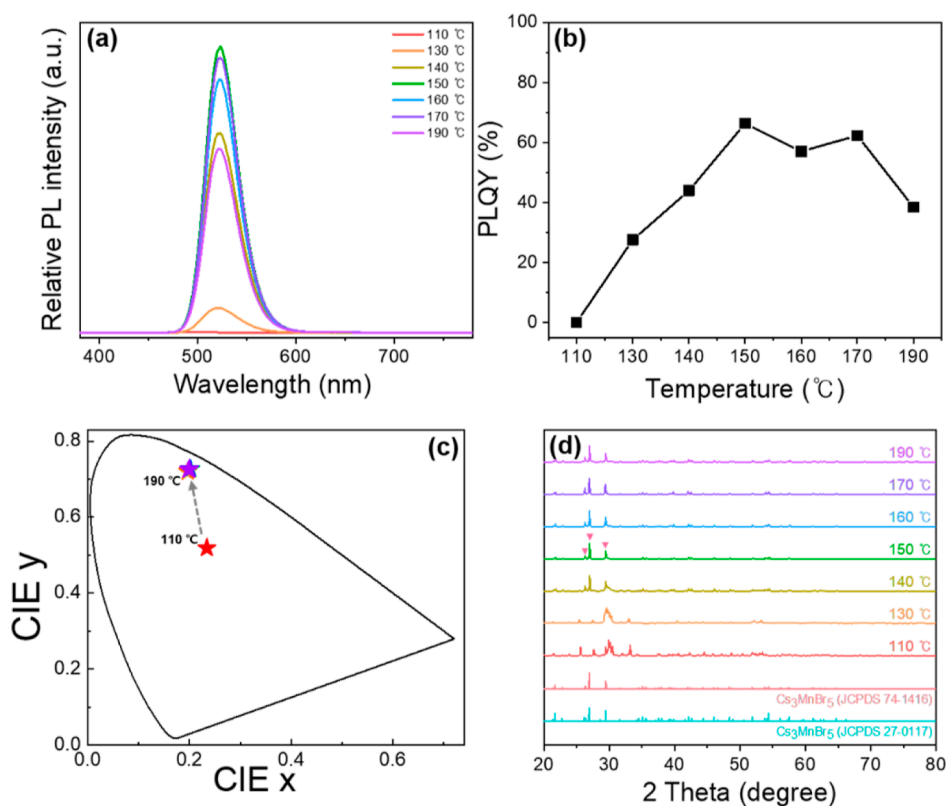

Figure 5. (a) PL spectra, (b) PLQY, (c) CIE color coordinates, and (d) XRD patterns of Cs_3MnBr_5 phosphors synthesized as a function of evaporative temperature, filtered using a 200 nm syringe filter.

certain impurities or secondary phases of Cs_2MnBr_4, $MnBr_2$, and unknown phases. XRD patterns having enhanced major peaks, indexed by (114), (213), and (204) planes of the 200 nm syringe-filtered Cs_3MnBr_5 phosphors, indicate that Cs_3MnBr_5 powder is better crystallized, with the tetragonal phase, than are unfiltered Cs_3MnBr_5 phosphors.[22] However, small amounts of certain residual phases remain after the optimum evaporative crystallization process (at 150 °C for 2
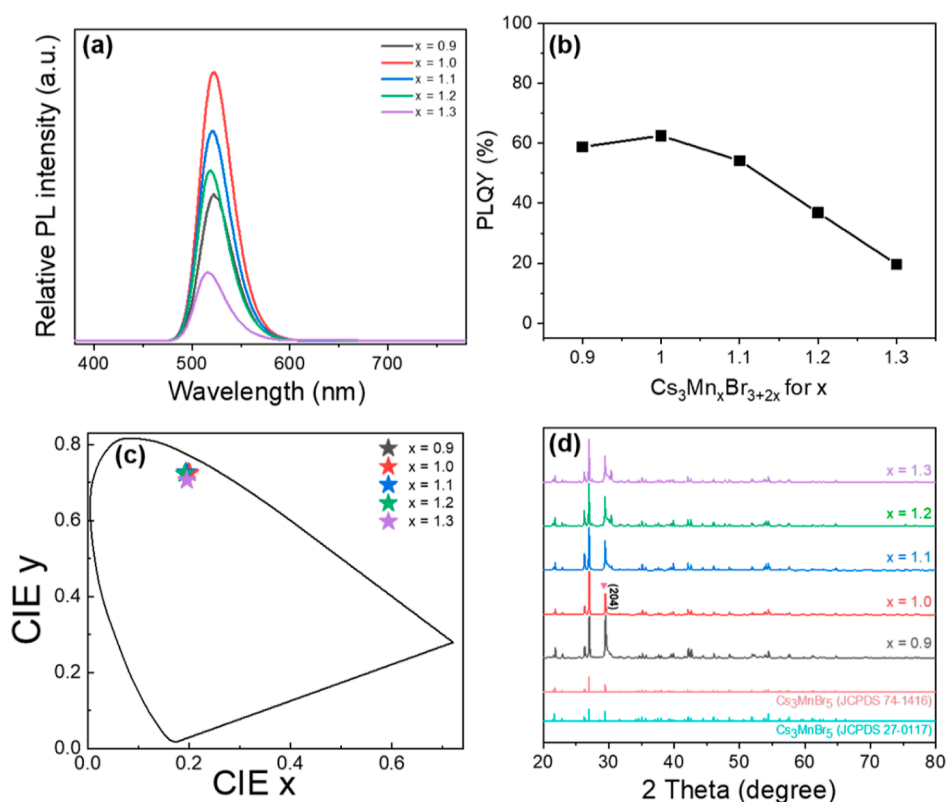
Figure 6. (a) PL spectra, (b) PLQY, (c) CIE color coordinates, and (d) XRD patterns of Cs_3MnBr_5 phosphors synthesized with variation of the compositional ratio.

h) of the purified reactant solutions. In terms of improving the PLQY or crystal quality of the synthesized Cs_3MnBr_5 powder phosphors, it will be necessary to further remove remaining impurities via the pre-filtration process before evaporative crystallization.

The SEM photographs (Figure 3b) of the non-filtered Cs_3MnBr_5 powders and of all of the filtered Cs_3MnBr_5 powders show morphologies that are similar in shape and agglomerated into nano-sized fine particles. EDS mapping measurements (Figure 3c) also indicate that Cs, Mn, and Br are evenly distributed for all four Cs_3MnBr_5 powders. EDS data also indicate that the better-filtered phosphor powder exhibits a phase with small amounts of elemental oxygen remaining, as shown in Figure 3d. As can be seen in the insets of Figure 4a, the color of the purified aqueous reactant solution becomes increasingly transparent with increased filtering. The photographs indicate that the purification process works effectively using any of the filters. Figure 4a also shows that the impurity absorption spectrum of the filtered solution decreases as the filtering effect increases. Absorption peaks indicate that the majority of impurities are removed, but small amounts of impurities remain in the purified solution even after purification by the syringe filter with the smallest pores. The XRD patterns in Figure 4b show mixed powder patterns for filtered impurities obtained from the surface of the 200 nm syringe filter. The SEM images in Figure 4c show that the filtered impurities have irregular shapes of agglomerated micro- and nanoparticles, with average sizes larger than the pore size of the syringe filter. EDS elemental analysis results shown in Figure 4d indicate that impurities consist of Mn, Cs, Br, and O elements in powders separated from solutions. Because oxygen is also detected in very small amounts in the filtered solids,

these impurities might be amorphous mixtures of Mn- and/or Cs-related oxides or hydroxides, as well as bromide, with average agglomerated size larger than the pore size of the syringe filter.[22] When a 200 nm syringe filter is used, oxygen impurities in the phosphor can be minimized.

We select the 200 nm syringe filter for purification of reactant solution for further optimization process. First, we optimize the optical quality of the as-synthesized Cs_3MnBr_5 powders by comparing the PLQYs and emission spectra of the as-synthesized Cs_3MnBr_5 powders as a function of evaporative temperature (Figure 5a,b). The resulting figures indicate that the best PLQY (66.3%) of Cs_3MnBr_5 powders is obtained by heating at 150 °C. Except for those of the Cs_3MnBr_5 powders synthesized at 110 °C, the PL spectrum and CIE color coordinates (Figure 5c) are almost identical in shape and position. XRD spectra also confirm that XRD patterns of the best PLQY Cs_3MnBr_5 powders are well matched with those of the standard Cs_3MnBr_5 phase (PDF card no. 71-1416, Figure 5c), with only minor impurity phases. Below 140 °C, with decreasing crystallization temperature, a phase transformation is observed from Cs_3MnBr_5 to mixed phases. This also indicates that crystal phases of powders are nearly identical in the crystallization temperature range of 150–190 °C.

Therefore, it is not easy to correlate the big changes of PLQY with the small peak changes found in the XRD patterns. It can be inferred that defects, which cannot be discerned by XRD and cause non-radiative recombination, greatly increase after the optimum evaporative temperature. As shown in Figure 5b,d, PLQY of the synthesized Cs_3MnBr_5 phosphors drops between 110 and 130 °C because Cs_3MnBr_5 phosphor crystals are not well formed. There is a correlation between the values of PLQY and fwhm of the (213) peak in the XRD

patterns of Cs_3MnBr_5 phosphors, synthesized from 140 to 190 °C, as shown in Figure S6. The greater the increase of the PLQY of the synthesized Cs_3MnBr_5 phosphors, the greater the decrease of the fwhm of the XRD maximum intensity peak. Therefore, we have chosen the evaporative temperature of 150 °C, which leads to the best PLQY of Cs_3MnBr_5 phosphors synthesized as a function of evaporative temperature and filtered using a 200 nm syringe filter. At temperatures between 150 and 190 °C, the body colors of all phosphors are similarly bright greenish; the phosphors also all emit bright G light under UV excitation (Figure S4). XRD results also show that the temperature dependence of the body color and light emission is not as sensitive as the change of PLQY. In the next step, PLQY was optimized according to the change in reaction time at 150 °C. The PL spectrum, CIE color coordinates, and PLQY graph in Figures S5 show that the best PLQY and best spectrum are obtained by heating at 150 °C for 2 h.

As a third step, we investigate the effect of the atomic ratio of Mn to Cs elements on the luminescence properties of $Cs_3Mn_xBr_{3+2x}$ phosphor powders. Although there are differences in the intensity of the spectra, the position and fwhm of the PL spectra show almost identical values even with variation of the compositional ratio, as shown in Figure 6a. The CIE color coordinates also show almost identical coordinate values of emitted light for the different composition ratios (Figure 6b). This confirms that the emission spectrum of $Cs_3Mn_xBr_{3+2x}$ phosphor powders is not significantly affected by the composition ratio; however, PLQY changes very sensitively. Figure 6c shows that PLQY decreases when the composition ratio of Cs/Mn deviates from 3:1. The XRD patterns (Figure 6d) also show that secondary impurity peaks appear in the Cs_3MnBr_5 crystal phase for the off-stoichiometric composition. At composition ratios of 3:0.9 and 3:1.1, a shoulder appears for the longer 2θ of the (204) main peak, and a secondary impurity peak also appears at ratios of 3:1.2 or higher. These results reconfirm that PLQY increases as the composition approaches the pure tetragonal phase of stoichiometric Cs_3MnBr_5 crystal structure.

3. CONCLUSIONS

In conclusion, we successfully developed eco-friendly Cs_3MnBr_5 powder phosphor as a G color-converting material using evaporative crystallization based on aqueous solution, an eco-friendly crystallization process using non-toxic solvent. As with the optimization process of synthesizing conventional inorganic phosphors, it is shown that reducing impurities in raw materials and increasing crystallinity of phosphor powders are the most important factors to increase the PLQY of Cs_3MnBr_5 phosphor powder. The brightest Cs_3MnBr_5 phosphor powder was obtained in an evaporative crystallization process by filtering aqueous mixed reactant solution with a 200 nm syringe filter and heating the filtered solution at a low temperature of 150 °C for a short reaction time of 2 h. Synthesized Cs_3MnBr_5 had optical properties of a PLQY of 66.3%, a peak wavelength of 520 nm, an fwhm of 38 nm, a decay time of 0.34 ms, and CIE color coordinates $x = 0.199$ and $y = 0.728$. Even though efficient and crystallized Cs_3MnBr_5 powders were synthesized by pre-filtered evaporative crystallization, a small portion of unknown impurities remained in the reactant solution, reducing the PLQY. Therefore, if any additional advanced purification process is to be developed in the future, impurity particles smaller than the pore size of the syringe filter will have to be completely removed before

crystallization. We suggest a simple method of synthesizing eco-friendly Cs_3MnBr_5 green phosphors through eco-friendly evaporative crystallization at low annealing temperature and short reaction time without using organic or acid solvents. In addition, we anticipate improved potential for realizing next-generation G light-emitting material for use in G color-converting layers in display applications.

4. METHODS

4.1. Materials. Cesium bromide (CsBr, 99.999%, Sigma-Aldrich), manganese(II) bromide ($MnBr_2$, 98%, Sigma-Aldrich), and distilled water.

4.2. Synthesis of Cs_3MnBr_5 Green Phosphors through Evaporative Crystallization. 0.09 mmol of CsBr, 0.03 mmol of $MnBr_2$, and distilled water were added to a beaker and heated and stirred at 60 °C for 30 min to ionize precursors. Then, the ionized reactant solution was filtered using various filtration conditions such as no filter, paper filter, a 450 nm syringe filter, and a 200 nm syringe filter to reduce impurities. The filtered ionized reactant solution was crystallized in a furnace at 150 °C for 2 h via evaporative crystallization. For further optimization, a 200 nm syringe filter for purification of reactant solution was synthesized as a function of crystallization temperature (110, 130, 140, 150, 160, 170, 190 °C) and via the $Cs_3Mn_xBr_{2+x}$ molar ratio ($x = 0.9$, 1.0, 1.1., 1.2., 1.3) for 2 h.

4.3. Characterization. The absorbance of filtered solutions was measured with a UV−vis spectrometer (S-3100, SINCO Co., Ltd.) PL and PLE spectra of the synthesized Cs_3MnBr_5 green phosphors were obtained with an Xe lamp and spectrophotometer (Darsa, PSI Trading Co., Ltd). PLQYs of the synthesized Cs_3MnBr_5 phosphors were measured in comparison with that of YAG:Ce^{3+} phosphor (absolute PLQY = 0.95 at 450 nm), measured using a TCSPC spectrofluorometer (Fluorolog 3, HORIBA). The TRPL spectra were measured using a home-made spectrometer. The synthesized Cs_3MnBr_5 phosphors were excited by the third harmonic of a nanosecond laser (SL I-20, Continuum) under ambient conditions. The emission was spectrally resolved using a monochromator, detected using a photomultiplier, and recorded using an oscilloscope (WAVE-SURFER 454, LeCroy). The crystal phases of the obtained Cs_3MnBr_5 green phosphors were characterized by XRD (Ultima IV, Rigaku). SEM (JSM-7610F, JEOL Ltd.) and EDS were utilized to analyze the size, morphology, crystal structure, elemental composition, and impurities of the synthesized Cs_3MnBr_5 green phosphors.

■ ASSOCIATED CONTENT

ⓈSupporting Information

The Supporting Information is available free of charge at https://pubs.acs.org/doi/10.1021/acsomega.2c00943.

> Detailed optical properties and photographs and EDS data of the synthesized Cs_3MnBr_5 phosphors with various filtration conditions and various crystallization temperatures (PDF)

■ AUTHOR INFORMATION

Corresponding Author

Young Rag Do − *Department of Chemistry, Kookmin University, Seoul 02707, Republic of Korea;* ⦿ orcid.org/0000-0002-0580-4628; Email: yrdo@kookmin.ac.kr

Authors

Sangwook Park − *Department of Chemistry, Kookmin University, Seoul 02707, Republic of Korea*

Minji Ko − *Department of Chemistry, Kookmin University, Seoul 02707, Republic of Korea*

Hyeng Jin Kim − *Department of Chemistry, Kookmin University, Seoul 02707, Republic of Korea*

Keyong Nam Lee − *Department of Chemistry, Kookmin University, Seoul 02707, Republic of Korea*

Complete contact information is available at:
https://pubs.acs.org/10.1021/acsomega.2c00943

Notes

The authors declare no competing financial interest.

■ REFERENCES

(1) Protesescu, L.; Yakunin, S.; Bodnarchuk, M. I.; Krieg, F.; Caputo, R.; Hendon, C. H.; Yang, R. X.; Walsh, A.; Kovalenko, M. V. Nanocrystals of Cesium Lead Halide Perovskites ($CsPbX_3$, X = Cl, Br, and I): Novel Optoelectronic Materials Showing Bright Emission with Wide Color Gamut. *Nano Lett.* **2015**, *15*, 3692−3696.

(2) Liu, F.; Zhang, Y.; Ding, C.; Kobayashi, S.; Izuishi, T.; Nakazawa, N.; Toyoda, T.; Ohta, T.; Hayase, S.; Minemoto, T.; Yoshino, K.; Dai, S.; Shen, Q. Highly Luminescent Phase-Stable $CsPbI_3$ Perovskite Quantum Dots Achieving Near 100% Absolute Photoluminescence Quantum Yield. *ACS Nano* **2017**, *11*, 10373−10383.

(3) Pan, J.; Shang, Y.; Yin, J.; De Bastiani, M.; Peng, W.; Dursun, I.; Sinatra, L.; El-Zohry, A. M.; Hedhili, M. N.; Emwas, A.-H.; Mohammed, O. F.; Ning, Z.; Bakr, O. M. Bidentate Ligand-Passivated $CsPbI_3$ Perovskite Nanocrystals for Stable Near-Unity Photoluminescence Quantum Yield and Efficient Red Light-Emitting Diodes. *J. Am. Chem. Soc.* **2018**, *140*, 562−565.

(4) Kovalenko, M. V.; Protesescu, L.; Bodnarchuk, M. I. Properties and Potential Optoelectronic Applications of Lead Halide Perovskite Nanocrystals. *Science* **2017**, *358*, 745−750.

(5) Yoon, H. C.; Lee, S.; Song, J. K.; Yang, H.; Do, Y. R. Efficient and Stable $CsPbBr_3$ Quantum-Dot Powders Passivated and Encapsulated with a Mixed Silicon Nitride and Silicon Oxide Inorganic Polymer Matrix. *ACS Appl. Mater. Interfaces* **2018**, *10*, 11756−11767.

(6) Zhu, Y.; Liang, Y.; Liu, S.; Li, H.; Chen, J. Narrow-Band Green-Emitting $Sr_2MgAl_{22}O_{36}:Mn^{2+}$ Phosphors with Superior Thermal Stability and Wide Color Gamut for Backlighting Display Applications. *Adv. Opt. Mater.* **2019**, *7*, 1801419.

(7) Song, E. H.; Zhou, Y. Y.; Wei, Y.; Han, X. X.; Tao, Z. R.; Qiu, R. L.; Xia, Z. G.; Zhang, Q. Y. A Thermally Stable Narrow-Band Green-Emitting Phosphor $MgAl_2O_4:Mn^{2+}$ for Wide Color Gamut Backlight Display Application. *J. Mater. Chem. C* **2019**, *7*, 8192−8198.

(8) Dong, Q.; Yang, F.; Cui, J.; Tian, Y.; Liu, S.; Du, F.; Peng, J.; Ye, X. Enhanced Narrow Green Emission and Thermal Stability in γ-AlON: Mn^{2+}, Mg^{2+} Phosphor via Charge Compensation. *Ceram. Int.* **2019**, *45*, 11868−11875.

(9) Zhang, S.; Liang, H.; Liu, Y.; Liu, Y.; Hou, D.; Zhang, G.; Shi, J. Intensive Green Emission of $ZnAl_2O_4:Mn^{2+}$ under Vacuum Ultraviolet and Low-Voltage Cathode Ray Excitation. *Opt. Lett.* **2012**, *37*, 2511−2513.

(10) Han, P.; Luo, C.; Yang, S.; Yang, Y.; Deng, W.; Han, K. All-Inorganic Lead-Free 0D Perovskites by a Doping Strategy to Achieve a PLQY Boost from <2 % to 90%. *Angew. Chem., Int. Ed.* **2020**, *59*, 12709−12713.

(11) Jiang, T.; Ma, W.; Zhang, H.; Tian, Y.; Lin, G.; Xiao, W.; Yu, X.; Qiu, J.; Xu, X.; Yang, Y.; Ju, D. Highly Efficient and Tunable Emission of Lead-Free Manganese Halides toward White Light-Emitting Diode and X-Ray Scintillation Applications. *Adv. Funct. Mater.* **2021**, *31*, 2009973.

(12) Xiao, H.; Dang, P.; Yun, X.; Li, G.; Wei, Y.; Wei, Y.; Xiao, X.; Zhao, Y.; Molokeev, M. S.; Cheng, Z.; Lin, J. Solvatochromic Photoluminescent Effects in All-Inorganic Manganese(II)-Based Perovskites by Highly Selective Solvent-Induced Crystal-to-Crystal Phase Transformations. *Angew. Chem., Int. Ed.* **2021**, *60*, 3699−3707.

(13) Hu, G.; Xu, B.; Wang, A.; Guo, Y.; Wu, J.; Muhammad, F.; Meng, W.; Wang, C.; Sui, S.; Liu, Y.; Li, Y.; Zhang, Y.; Zhou, Y.; Deng, Z. Stable and Bright Pyridine Manganese Halides for Efficient White Light-Emitting Diodes. *Adv. Funct. Mater.* **2021**, *31*, 2011191.

(14) Zhou, G.; Liu, Z.; Huang, J.; Molokeev, M. S.; Xiao, Z.; Ma, C.; Xia, Z. Unraveling the Near-Unity Narrow-Band Green Emission in Zero-Dimensional Mn^{2+}-Based Metal Halides: A Case Study of $(C_{10}H_{16}N)_2Zn_{1−x}Mn_xBr_4$ Solid Solutions. *J. Phys. Chem. Lett.* **2020**, *11*, 5956−5962.

(15) Ma, Y.-Y.; Song, Y.-R.; Xu, W.-J.; Zhong, Q.-Q.; Fu, H.-Q.; Liu, X.-L.; Yue, C.-Y.; Lei, X.-W. Solvent-free mechanochemical syntheses of microscale lead-free hybrid manganese halides as efficient green light phosphors. *J. Mater. Chem. C* **2021**, *9*, 9952−9961.

(16) Su, B.; Molokeev, M. S.; Xia, Z. Mn^{2+}-Based narrow-band green-emitting Cs_3MnBr_5 phosphor and the performance optimization by Zn^{2+} alloying. *J. Mater. Chem. C* **2019**, *7*, 11220−11226.

(17) Kwon, S. B.; Choi, S. H.; Yoo, J. H.; Kim, B. Y.; Kang, B. K.; Song, Y. H.; Yoon, D. H. Organic Solvent-Free Lyophilization Assisted Recrystallization Synthesis of High-Purity Green Emissive Cs_3MnX_5 (X = I, Br). *J. Alloys Compd.* **2020**, *845*, 156324.

(18) Kong, Q.; Yang, B.; Chen, J.; Zhang, R.; Liu, S.; Zheng, D.; Zhang, H.; Liu, Q.; Wang, Y.; Han, K. Phase Engineering of Cesium Manganese Bromides Nanocrystals with Color-Tunable Emission. *Angew. Chem., Int. Ed.* **2021**, *60*, 19653−19659.

(19) Shao, L.; Zhou, D.; Ding, N.; Sun, R.; Xu, W.; Wang, N.; Xu, S.; Liu, D.; Song, H. Broadband Ultraviolet Photodetectors Based on Cerium Doped Lead-Free Cs_3MnBr_5 Metal Halide Nanocrystals. *ACS Sustainable Chem. Eng.* **2021**, *9*, 4980−4987.

(20) Kubicki, D. J.; Prochowicz, D.; Pinon, A.; Stevanato, G.; Hofstetter, A.; Zakeeruddin, S. M.; Grätzel, M.; Emsley, L. Doping and Phase Segregation in Mn^{2+}- and Co^{2+}-Doped Lead Halide Perovskites from ^{133}Cs and ^1H NMR Relaxation Enhancement. *J. Mater. Chem. A* **2019**, *7*, 2326−2333.

(21) Almutlaq, J.; Mir, W. J.; Gutiérrez-Arzaluz, L.; Yin, J.; Vasylevskyi, S.; Maity, P.; Liu, J.; Naphade, R.; Mohammed, O. F.; Bakr, O. M. $CsMnBr_3$: Lead-Free Nanocrystals with High Photoluminescence Quantum Yield and Picosecond Radiative Lifetime. *ACS Mater. Lett.* **2021**, *3*, 290−297.

(22) Kim, H. J.; Ko, M.; Park, S.; Lee, K. N.; Yoo, G. Y.; Nam, S.; Song, J. K.; Do, Y. R. Fabrication of SiN_x Nanopore Filters Using Combined Process of Nanoimprint and Dual-Side Aligned Photolithography for Purified Cs_3MnBr_5 Green Phosphors. *Adv. Mater. Technol.* **2022**, 2101519.

(23) Gong, L.-K.; Hu, Q.-Q.; Huang, F.-Q.; Zhang, Z.-Z.; Shen, N.-N.; Hu, B.; Song, Y.; Wang, Z.-P.; Du, K.-Z.; Huang, X.-Y. Efficient Modulation of Photoluminescence by Hydrogen Bonding Interactions between Inorganic $[MnBr_4]^{2-}$ Anions and Organic Cations. *Chem. Commun.* **2019**, *55*, 7303.

(24) Morad, V.; Cherniukh, I.; Pöttschacher, L.; Shynkarenko, Y.; Yakunin, S.; Kovalenko, M. V. Manganese(II) in Tetrahedral Halide Environment: Factors Governing Bright Green Luminescence. *Chem. Mater.* **2019**, *31*, 10161−10169.

(25) Morad, V.; Cherniukh, I.; Pöttschacher, L.; Shynkarenko, Y.; Yakunin, S.; Kovalenko, M. V. Manganese(II) in Tetrahedral Halide Environment: Factors Governing Bright Green Luminescence. *Chem. Mater.* **2019**, *31*, 10161−10169.

(26) Allard, S.; Fouche, L.; Dick, J.; Heitz, A.; von Gunten, U. Oxidation of Manganese(II) during Chlorination: Role of Bromide. *Environ. Sci. Technol.* **2013**, *47*, 8716−8723.